



## King's Research Portal

*Document Version*  
Peer reviewed version

[Link to publication record in King's Research Portal](#)

*Citation for published version (APA):*

Weber, C. (in press). Study of disorder in pulsed laser deposited double perovskite oxides by first-principle structure prediction. *Nature Computational Materials*.

### **Citing this paper**

Please note that where the full-text provided on King's Research Portal is the Author Accepted Manuscript or Post-Print version this may differ from the final Published version. If citing, it is advised that you check and use the publisher's definitive version for pagination, volume/issue, and date of publication details. And where the final published version is provided on the Research Portal, if citing you are again advised to check the publisher's website for any subsequent corrections.

### **General rights**

Copyright and moral rights for the publications made accessible in the Research Portal are retained by the authors and/or other copyright owners and it is a condition of accessing publications that users recognize and abide by the legal requirements associated with these rights.

- Users may download and print one copy of any publication from the Research Portal for the purpose of private study or research.
- You may not further distribute the material or use it for any profit-making activity or commercial gain
- You may freely distribute the URL identifying the publication in the Research Portal

### **Take down policy**

If you believe that this document breaches copyright please contact [librarypure@kcl.ac.uk](mailto:librarypure@kcl.ac.uk) providing details, and we will remove access to the work immediately and investigate your claim.

# Study of disorder in pulsed laser deposited double perovskite oxides by first-principle structure prediction

Edoardo Fertitta<sup>a),1</sup>, Sujit Das,<sup>2</sup> Debalina Banerjee,<sup>3</sup> Farbod Ebrahimi,<sup>1</sup> Clément Barraud,<sup>4,1</sup> Kai Du,<sup>5</sup> He Tian,<sup>5</sup> Chris J. Pickard,<sup>6,7</sup> Cedric Weber,<sup>3,1</sup> Ramamoorthy Ramesh,<sup>2</sup> Peter Littlewood,<sup>8</sup> and David Dubbink<sup>1</sup>

<sup>1</sup>*Happy Electron Ltd, London W3 7XS, United Kingdom*

<sup>2</sup>*Department of Materials Science and Engineering, University of California, Berkeley, California 94720, USA*

<sup>3</sup>*Department of Physics, King's College London, London WC2R 2LS, United Kingdom*

<sup>4</sup>*Laboratoire Matériaux et Phénomènes Quantiques, UMR 7162, Université de Paris, CNRS, 75013 Paris, France*

<sup>5</sup>*Center of Electron Microscopy, School of Materials Science and Engineering, Zhejiang University, Hangzhou, 310027, China*

<sup>6</sup>*Department of Materials Science and Metallurgy, Cambridge CB3 0FS, United Kingdom*

<sup>7</sup>*Advanced Institute for Materials Research, Tohoku University, Sendai, 980-8577, Japan*

<sup>8</sup>*James Franck Institute and Department of Physics, University of Chicago, Chicago IL 60637, USA*

Double perovskite oxides, with generalised formula  $A_2BB'O_6$ , attract wide interest due to their multiferroic and charge transfer properties. They offer a wide range of potential applications such as spintronics and electrically tunable devices. However, great practical limitations are encountered, since a spontaneous order of the B-site cations is notoriously hard to achieve. In this joint experimental-theoretical work, we focused on characterisation of double perovskites  $La_2TiFeO_6$  and  $La_2VCuO_6$  films grown by pulsed laser deposition and interpretation of the observed B-site disorder and partial charge transfer between the B-site ions. A random structure sampling method was used to show that several phases compete due to their corresponding configurational entropy. In order to capture a representative picture of most relevant competing microstates in realistic experimental conditions, this search included the potential formation of non-stoichiometric phases as well, which could also be directly related to the observed partial charge transfer. We optimised the information encapsulated in the potential energy landscape, captured via structure sampling, by evaluating both enthalpic and entropic terms. These terms were employed as a metric for the competition of different phases. This approach, applied herein specifically to  $La_2TiFeO_6$ , highlights the presence of highly entropic phases above the ground state which can explain the disorder observed frequently in the broader class of double perovskite oxides.

Keywords: Double perovskite oxides | First principle structure prediction | Random structure sampling | Entropy forming ability | Pulsed Laser Deposition | DFT+U | Charge transfer

Double perovskite oxides  $A_2BB'O_6$ , in which the B-sites of the unit cell are occupied by different transition metal cations, exhibit a wide range of magnetic and transport properties, ranging from ionic conductivity<sup>1</sup>, superconductivity<sup>2</sup>, to ferromagnetism<sup>3,4</sup>, ferroelectricity<sup>5,6</sup> and multiferroic behavior<sup>7</sup>. Tuning these properties by changes in structure and nature of the A- and B-site cations suggests a variety of potential applications such as magnetic refrigeration<sup>8</sup>, and magneto-optic<sup>9</sup> and photovoltaic devices<sup>10</sup>. The properties of these type of materials can depend heavily on the ordering of the B-site cations. For example, the double perovskite  $La_2MnNiO_6$  is a ferromagnet when Ni and Mn are rocksalt ordered at the perovskite B-site, while randomly distributed Mn and Ni gives rise to antiferromagnetic correlations<sup>11</sup>. This is particularly important from the perspective of synthesis. While many interesting properties have been predicted for B-site ordered double perovskite, only few have been realised experimentally<sup>12,13</sup>, mainly limited to double perovskites containing B-site ions with large differences in cation size or valency<sup>14,15</sup>. The aim of this work is to investigate the mechanisms behind the difficulties to realise B-site order in perovskite systems, even if an ordered state is thermodynamically favored at first sight<sup>16</sup>.

This work focuses on two double perovskites containing different 3d transition metals at the B-site, namely  $La_2TiFeO_6$  and  $La_2VCuO_6$ . These materials have in common charge transfer (CT) processes between the B-site ions<sup>17</sup> that can lead to different transition metal oxidation state pairs, i.e.  $Fe^{3+}/Ti^{3+}$  and  $Fe^{2+}/Ti^{4+}$ ,  $Cu^{2+}/V^{4+}$  and  $Cu^+/V^{5+}$ , and correspondingly to different properties. It is tempting to create the conditions allowing for reversible control of these charge transfer processes. In a recent study<sup>18</sup>, we predicted via density functional theory (DFT)+U that the charge transfer between Fe and Ti in  $LaTiO_3/LaFeO_3$  heterostructures strained on  $SrTiO_3$  and  $LaAlO_3(100)$  substrates varies sensibly as a function of internal pressure. Also, in this system the charge-transfer mechanism is associated to a tunable ferroelectric behavior since a net polarization of the LaO plane can be created or destroyed as a function of the nominal charge of the  $TiO_2$  and  $FeO_2$  planes.  $La_2VCuO_6$  also offers interesting possible applications as it is a potential half metal when V and Cu are respectively in the 4+

<sup>a)</sup> Corresponding author: edoardo.fertitta@he.co

and 2+ oxidation state and an insulator when V and Cu are respectively 5+ and 1+<sup>19</sup>, offering the opportunity to induce a metal-insulator transition by controlling the charge transfer process. However, to our knowledge neither material has been realised experimentally in their B-site ordered double perovskite form, which could be detrimental to the envisioned properties.

This work is dedicated to realization of B-site ordered double perovskite oxides. Pulsed Laser Deposition (PLD) was used to grow  $\text{La}_2\text{TiFeO}_6$  and  $\text{La}_2\text{VCuO}_6$  on  $\text{SrTiO}_3$  (100) and (111) substrates in order to epitaxially stabilise the perovskite phase and potentially use strain to enhance the B-site order<sup>20</sup>. Although high crystalline quality epitaxial perovskite films were made, our experiments confirmed the difficulty of obtaining B-site ordering, which was absent in all our films. In order to guide the design of a controlled growth, an in-depth interpretation of experimental data by high-fidelity modelling becomes necessary. Therefore, the major part of this work is a detailed computational ab-initio study towards the occurrence of disorder in these double perovskites. During growth of the materials, a plethora of structures may compete, and defects can change the energy landscape significantly. This cannot be addressed by searching the ground state of the materials among a few possible candidates, and requires an in-depth exploration of the energy landscape.

Several computational approaches have been successfully applied to the computational sampling of thermodynamically stable compounds, all involving a search for the low-lying energy minima in a high-dimensional configuration space. Evolutionary algorithms such as the Oganov–Glass<sup>21</sup> and Wang’s version of particle swarm optimisation<sup>22</sup> are particularly popular. These are based on the idea that a population of structures is evolved by penalising or favouring certain phases as a function of their energy. A different route is taken by random structure sampling methods popularised by implementations such as USPEX<sup>23,24</sup>, CALYPSO<sup>25</sup> and the Ab-Initio Random Structure Search (AIRSS)<sup>26–28</sup>, which is employed in this investigation. This approach is based upon the structural optimisation of randomly generated structures within chemically intuitive constraints to reduce the size of the explored phase space. The great advantage of such an implementation is its intrinsically highly parallelisability as individual structure relaxations do not depend on each other. Despite its potential high computational cost, the AIRSS method has been applied successfully, for example leading to the discovery of new high pressure phases such as solid hydrogen<sup>29</sup> and ionic ammonia<sup>30</sup>.

Random structure sampling offers the unique advantage of generating more scientific information than characterisation of low-lying states only. In fact, this procedure allows for the mapping of the entire energy landscape, given that the applied constraints allow for it. Therefore, AIRSS lends itself to the handling of configurational entropy<sup>31</sup> if significantly large statistics are collected. The configurational entropy is connected to the size of the basin of attraction of the found structure, which in turn is reflected by the frequency of occurrence of relevant structures<sup>32–37</sup>. The entropic term is also reflected by the density of the energy spectrum which can be evaluated via the entropy forming ability (EFA)<sup>38</sup>. This formalism has been utilised in the past to classify high entropy alloys and predict their relative thermodynamic stability. Herein, the formalism is applied to calculate the amount of competing phases in certain energy window over the whole spectrum, in order to compare the entropy of different structure in the same phase space. Although both these metrics do not capture the role of the vibrational entropy which might be important at higher temperatures, they yield reasonable arguments for the classification of different phases based on their enthalpic and entropic terms.

The computational study of both ground state and growth temperature activated states (within a few hundreds meV from ground state) reveals the presence of competing highly entropic phases above the ground state. These are thought to be responsible for a rich polymorphism leading to the B-site disorder observed via experimental characterisation. Also, the inclusion of different stoichiometries in the computational exploration of the phase space allowed us to explore the role of defects formation on the number of competing phases. Finally, analysis of the distribution of magnetic moments over the whole spectrum revealed how the stoichiometry can affect the magnetic order as well.

## RESULTS AND DISCUSSION

### Films characterisation

As described in the materials and methods section, pulsed laser deposition was used to grow  $\text{La}_2\text{TiFeO}_6$  and  $\text{La}_2\text{VCuO}_6$  films on both (001) and (111) oriented  $\text{SrTiO}_3$  substrates. The crystalline structure of the films were examined in detail by X-ray diffraction (XRD). As shown in Fig. 1(a), the  $\theta - 2\theta$  scan of an  $\text{La}_2\text{TiFeO}_6$  film on a STO (001) substrate indicated presence of a single perovskite phase. The symmetry of the unit cell was investigated by means of reciprocal space mapping. As shown in Fig. 1(e), the  $\text{La}_2\text{TiFeO}_6$  film was epitaxially strained to the  $\text{SrTiO}_3$ (001) substrate and had a tetragonal symmetry with  $a=b=3.91 \text{ \AA}$ , and  $c=4.01 \text{ \AA}$ . The high crystalline quality of the film was confirmed by AFM, since a step-and-terrace surface morphology was clearly visible with height differences corresponding to half an unit cell of the double perovskite (Fig. 1(c)). Similar results were obtained for  $\text{La}_2\text{VCuO}_6$  films on STO (001) substrates, as shown in more detail in Supplementary Information Fig. S2. The lattice parameters of the  $\text{La}_2\text{VCuO}_6$  tetragonal cell were  $a=b=3.91 \text{ \AA}$  and  $c=3.97 \text{ \AA}$ .

Although the films were clearly perovskites, absence of higher order peaks in the XRD  $\theta - 2\theta$  scans suggested a random distribution of Ti and Fe (and Cu and V) on the B-site of the perovskite unit cell. The higher order peaks were absent on both (001) and (111) oriented substrates, in both in- and out-of-plane scans, confirming neither planar nor rock-salt ordering of the

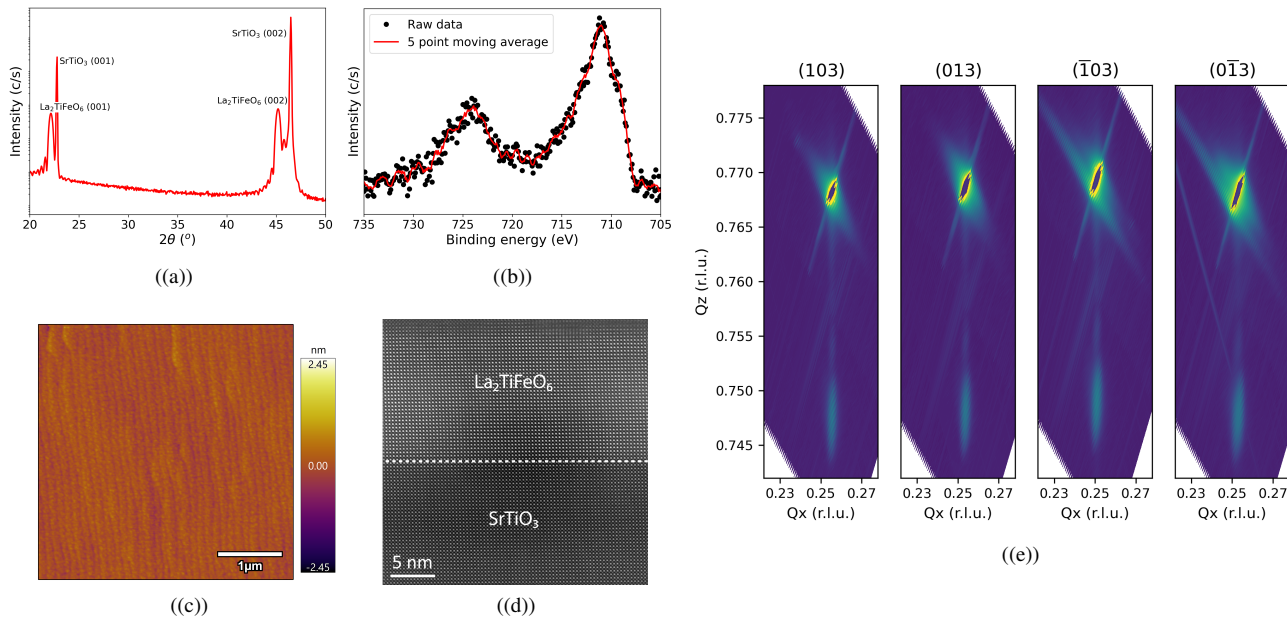


FIG. 1: Characterisation of a  $\text{La}_2\text{TiFeO}_6$  film on a  $\text{SrTiO}_3$  (001) substrate. XRD (a) shows peaks corresponding to single phase perovskite  $\text{La}_2\text{TiFeO}_6$ , but peaks indicating B-site ordering of Ti and Fe are absent. XPS (b) shows presence of  $\text{Fe}^{2+}$  in (001) oriented films, and is visible as a shoulder around 709 eV. XPS additionally shows Ti is completely 4+ (data not included). (c) AFM measurements show smooth films with terrace height differences of 0.5 unit cells. Also TEM (d) reveals a high structural quality of the grown films and absence of B-site order. (e) XRD reciprocal space mapping around the (103) reflection reveals that the strained film exhibit tetragonal symmetry with cell parameters  $a=3.905 \text{ \AA}$  and  $c=4.01 \text{ \AA}$ .

106 B-site cations occurred in any of the films. The absence of higher order peaks in out-of-plane scans of thin films on the (001)  
 107 oriented substrates confirmed the absence of planar ordering (see Fig. 1(a)). The potential rocksalt ordering on (001) oriented  
 108 substrates was addressed by performing scans in the [111] direction. Additionally, films were grown on (111) oriented substrates,  
 109 where any rocksalt would be observable in out-of-plane scans. In both cases, absence of higher order peaks excluded presence  
 110 of any rocksalt ordering (see Supplementary Information Fig.S1 and S2) The high structural quality and absence of B-site order  
 111 where confirmed by Scanning Transmission Electron Microscopy (STEM), as shown in Fig. 1(d).

112 Finally, the oxidation states of Fe and Ti were examined by means of X-ray Photoelectron Spectroscopy (XPS). The spectrum  
 113 of the (001) oriented  $\text{La}_2\text{TiFeO}_6$  film shown in Fig. 1(b) reveals that the Fe ions are partly in the 2+ oxidation state, while Ti is  
 114 completely 4+ (data not shown). The deviation from the expected  $\text{Fe}^{3+}$  in  $\text{LaFeO}_3$  and  $\text{Ti}^{3+}$  in  $\text{LaTiO}_3$  confirms the occurrence  
 115 of charge transfer from Ti to Fe when combining these materials in a (B-site disordered) double perovskite. The XPS spectra are  
 116 comparable to previously published work on  $\text{LaTiO}_3/\text{LaFeO}_3$  heterostructures<sup>39</sup>. In both cases, charge transfer leads to partial  
 117 reduction of the Fe, while a higher degree of reduction is expected based on the complete oxidation of Ti and the predicted  
 118 electronic structure by DFT<sup>18,39</sup>. In the  $\text{La}_2\text{TiFeO}_6$  films grown in this work, complete oxidation of Ti could lead to a complete  
 119 reduction of Fe due to the 1:1 ratio of Fe:Ti. The fact that Ti is completely 4+, while only part of the Fe is 2+, highlights that other  
 120 phenomena beyond the Ti to Fe charge transfer must be responsible for the oxidation of titanium ions. Possible explanations  
 121 might involve overoxidation during or post growth and La-vacancies

122 Both B-site disorder and partial charge transfer may prevent any application of these charge transfer processes. Note that  
 123 an exhaustive growth study was not performed in this work, and investigation of a much wider growth parameter space needs  
 124 to be addressed to make firm conclusions about the question whether or not it would be possible to obtain the ordered double  
 125 perovskites. However, the experimental results are exemplary for a wide range of published results of attempts to grow B-site  
 126 ordered double perovskites<sup>13</sup>.

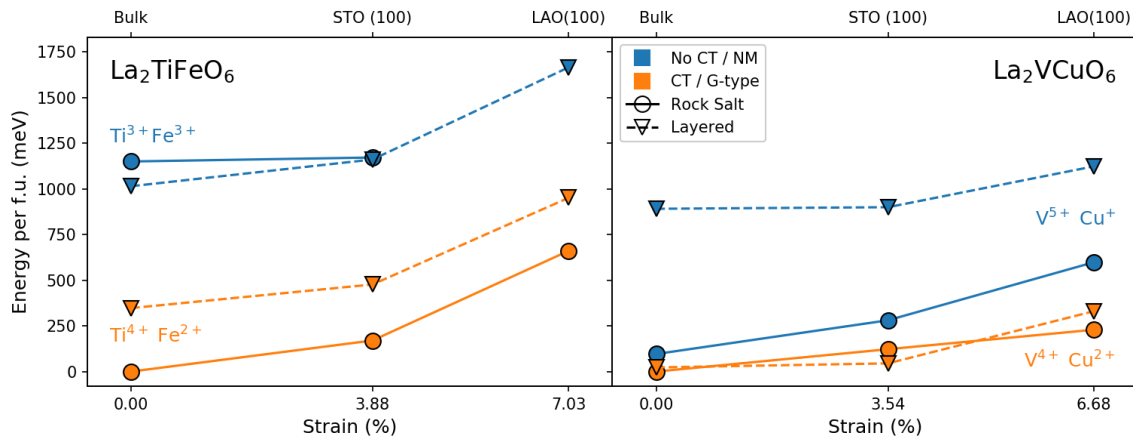


FIG. 2:  $\text{La}_2\text{TiFeO}_6$  and  $\text{La}_2\text{VCuO}_6$  energy per formula unit of the different states investigated for rock-salt and layered B-site ordering, for bulk phase and for phases strained to  $\text{SrTiO}_3$  and  $\text{LaAlO}_3(100)$  oriented substrates. Charge transfer and non-charge transfer states are shown for  $\text{La}_2\text{TiFeO}_6$  while G-type and non magnetic states are shown for  $\text{La}_2\text{VCuO}_6$ .

## 127 Simulations

### 128 Ordered phases

129 In order to investigate the possible causes of the observed B-site disorder we employed DFT to study the competition of  
 130 different phases. In this section we will focus on the theoretical investigation of some representative B-site ordered phases.  
 131 As detailed in the materials and methods section, DFT+U was used to model the strained  $\text{La}_2\text{TiFeO}_6$  and  $\text{La}_2\text{VCuO}_6$  films in  
 132 rock salt and layered phases. Different initial magnetic configurations were chosen in order to stabilise the different (non) CT  
 133 phases, as detailed more in previous work<sup>18</sup>.

134 As previously reported<sup>18</sup>, the ground state of  $\text{La}_2\text{TiFeO}_6$  is characterised by  $\text{Fe}^{2+}$  high spin and  $\text{Ti}^{4+}$  oxidation states. This  
 135 is a CT state as formal oxidation states in the  $\text{LaFeO}_3$  and  $\text{LaTiO}_3$  building blocks are  $\text{Fe}^{3+}$  and  $\text{Ti}^{3+}$ , respectively. Minima  
 136 corresponding to both the CT and non-CT state could be identified by DFT+U for different levels of strain, presenting the  
 137 same  $a^-b^-c^+$  octahedral rotations as the  $\text{LaFeO}_3$  and  $\text{LaTiO}_3$  building blocks. Differently, in the  $\text{La}_2\text{VCuO}_6$  case, the nominal  
 138  $\text{Cu}^{3+}$  and  $\text{V}^{3+}$  states of bulk  $\text{LaCuO}_3$  and  $\text{LaVO}_3$  could not be stabilised in any of the searched minima. Instead, two  $\text{V} \rightarrow \text{Cu}$   
 139 charge transfer states were found. After screening different magnetic orders (see Fig. ?? of the Supplementary Information), we  
 140 identified the ground state as G-type  $\text{Cu}^{2+}/\text{V}^{4+}$  both for rock-salt and layered orders with the same  $a^-b^-c^+$  octahedral rotations  
 141 as  $\text{LaVO}_3$ . An additional one-electron transfer leads to a non-magnetic state with formal  $\text{V}-d^0$  and  $\text{Cu}-d^{10}$ . These competing  
 142 states had been previously investigated by means of DFT+U<sup>19</sup>, predicting the  $\text{Cu}^{2+}/\text{V}^{4+}$  state to be a half metal for certain  
 143 choices of U. However, in our case a sensible gap is opened since octahedral rotations are taken into account, while the gap is  
 144 only reduced when octahedral rotations are suppressed (data not shown).

145 In order to explore the effect of substrate strains on the relative stability of these different phases and states and hence to  
 146 predict how these affect the one-electron CT  $\text{B} \rightarrow \text{B}'$  energy gap, we modelled different epitaxially strained phases as described in  
 147 the materials and methods section. In Fig. 2 we report the energy per formula unit of all  $\text{La}_2\text{TiFeO}_6$  and  $\text{La}_2\text{VCuO}_6$  fully relaxed  
 148 cells calculated for bulk phases and for epitaxially strained phases to model the growth on  $\text{SrTiO}_3$  and  $\text{LaAlO}_3$  substrates. In  
 149 the  $\text{La}_2\text{TiFeO}_6$  case, the CT state in the rock-salt order is always the most stable configuration, irrespective of the applied strain,  
 150 and the layered CT state is 200-300 meV above it. Differently, the  $\text{La}_2\text{VCuO}_6$  G-type ground state shows competition between  
 151 the rock-salt and layered order within 10 meV per atom and this separation is only slightly enhanced by strain on  $\text{LaAlO}_3(100)$   
 152 substrate. This is reflected by the fact that there is a smaller change in the size of the octahedra between the two structures for  
 153  $\text{La}_2\text{VCuO}_6$  than for  $\text{La}_2\text{TiFeO}_6$  (see Table ?? in the Supplementary Information). The gap between the  $\text{Cu}^{2+}/\text{V}^{4+}$  and  $\text{Cu}^+/\text{V}^{5+}$   
 154 exhibit a quite clear phase and strain dependence. Indeed, in the case of rock-salt order it doubles from 200 meV to 400 meV  
 155 as a function of strain, while it ranges around 800 meV for all structures in the case of a layered order. This can be explained  
 156 considering the differences in the ionic radii.  $\text{Cu}^+$  is about 25 pm larger than  $\text{V}^{5+}$ , giving rise to increased strain on the Cu  
 157 and V octahedra in case of the layered structure<sup>16</sup> (see Table ??). On the other hand, the difference between Cu and V ions is  
 158 reduced for  $\text{Cu}^{2+}$  and  $\text{V}^{4+}$  making the layered and rock-salt phases more competitive. In  $\text{La}_2\text{TiFeO}_6$  the situation is similar for  
 159 the layered phase, where a large charge transfer gap of 600 meV is observed. However, the CT rock-salt phase is sensibly more  
 160 stable than the layered one. This cannot be understood in terms of ionic radii alone as Fe and Ti are quite comparable in size.

161 The predicted competition between rock-salt and layered orders in  $\text{La}_2\text{VCuO}_6$  justifies the experimentally observed absence

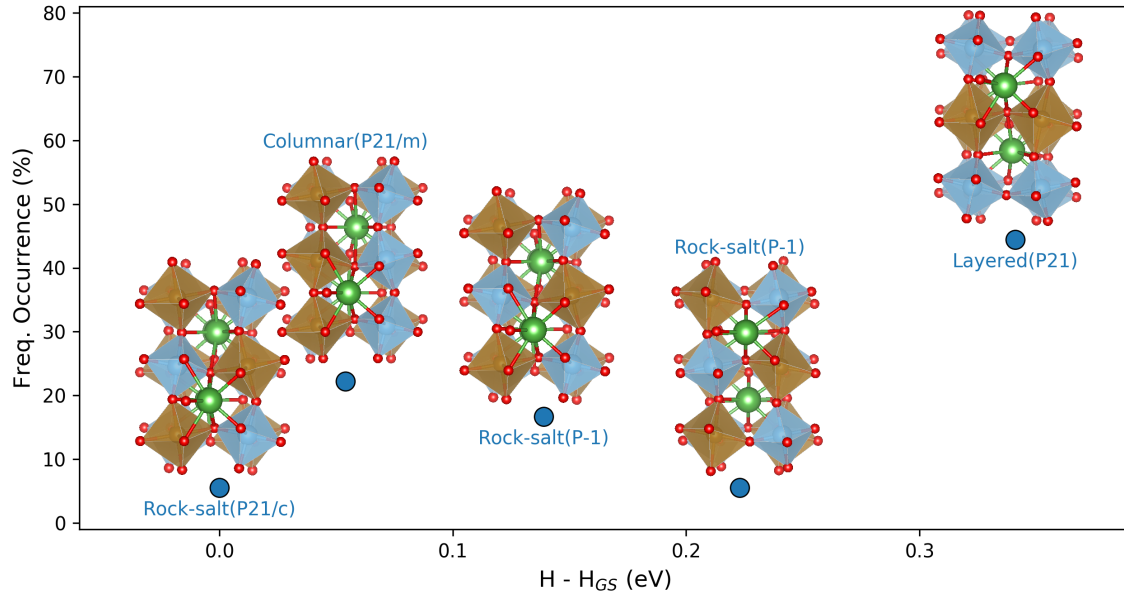


FIG. 3: Frequency of occurrence of  $\text{La}_2\text{TiFeO}_6$  perovskite structures captured by AIRSS within 400 meV of the ground state. The rock-salt with symmetry  $P_{21}/C$  was found to occur less often than the columnnar and layered phases. Above 100 meV other rock-salt phases with reduced symmetry and different octahedral rotations were found. The competition of these phases and the higher entropy associated with the more frequently occurring phases aligns with the experimentally observed disorder. In the reported structures, the atoms are labelled with different colors: green for La, red for O, blue for Ti and brown for Fe.

162 of B-site order. Note that controlled formation of  $\text{Cu}^+/\text{V}^{5+}$  could favor growth of the rocksalt ordered structure, in agreement  
 163 with the phase diagram proposed by Ohtomo *et al*<sup>15</sup>.

164 The observed disorder is harder to explain for  $\text{La}_2\text{TiFeO}_6$  on the basis of these results, as the predicted CT phases do not  
 165 show any competition. Moreover, the presence of majority of  $\text{Fe}^{3+}$  in the grown films cannot be understood from the reported  
 166 calculations alone, since the  $\text{Fe}^{2+}/\text{Ti}^{4+}$  phases are considerably more stable compared to the  $\text{Fe}^{3+}/\text{Ti}^{3+}$  phases. It becomes  
 167 necessary to investigate more phases which might contribute to the disordered growth. Also, defects such as lanthanum vacancies  
 168 and the presence of extra oxygen must be included in structure search as they might be responsible of the observed  $\text{Fe}^{2+}:\text{Fe}^{3+}$   
 169 ratio.

### 170 *Random structure search*

171 In order to perform this search, the ab-initio random structure search (AIRSS) method was employed. Exploring the vast  
 172 phase space by means of such a random sampling approach gives us the chance to reveal phases that might be missed by  
 173 structural optimisation of cells constructed based on chemical intuition. Sampling statistically significant structures via a fast  
 174 exploration of a vast fraction of phase space will allow to extract thermodynamical meaningful information to understand the  
 175 nature of the grown films. Although, this will not allow for a description of kinetics of the PLD growth process, characterising  
 176 the thermodynamically competing phases will lead to describe the driving force dominating during cooling which leads to B-  
 177 site (dis)order<sup>20</sup>. Indeed, during PLD growth, the high-energy adatoms have diffusion lengths of tens of nanometres which are  
 178 sufficient to make them migrate and stick to thermodynamically favourable positions. Hence, the grown film will be constituted  
 179 by a mixture of competing phases contributing to a rich polymorphism or disorder depending on the domain sizes. Since  
 180 a quantitative calculation of the phase domain sizes goes beyond the scope of this study, in the remainder of the paper we  
 181 simply will refer to disorder. Also, the information captured by sampling the phase space allows one to explore the role of  
 182 configurational entropy as well, which yields an additional argument to understand the competition of different microstates  
 183 which compose disordered structures. Herein, we employ two approaches to qualitatively capture this information, i.e. the  
 184 relative frequency of occurrence of different phases and the entropy forming ability (EFA).

185 The first argument is intrinsically connected to the random nature of the structure sampling approach, which in this respect  
 186 offers a more thermodynamical representation than structure learning based methods. Indeed, frequencies of occurrence of

187 phases obtained by a random sampling search can be related to the volume of the basins of attraction of such minima<sup>32-37</sup>, which  
 188 expresses how accessible these phases are and gives an indication of the configurational entropy. In Fig. 3, the relative frequency  
 189 of occurrence of the phases within 400 meV of the ground state are shown together with their structures, as predicted by the  
 190 AIRSS method. In this energy window, five minima were identified, all corresponding to B-site ordered perovskite structures.  
 191 The rock-salt and layered phases with octahedral rotations  $a^-b^-c^+$  described in the previous section were found, and the ground  
 192 state was predicted to be the rock-salt ordered structure in correspondence to our original structural optimisation. Additionally, a  
 193 columnar ordered phase was found 50 meV above the rock-salt phase, followed by other distorted rock-salt phases with different  
 194 octahedral rotations ( $a^-b^-c^-$ ). These findings already add substantial information to the partial picture we depicted in Fig. 2, as  
 195 the competing phases naturally contribute to the observed B-site disorder.

196 In addition to the observation of additional phases, a more complex picture emerges from their frequency of occurrence, since  
 197 the minima above the rock-salt ground state are associated to larger basins of attraction. Similar to the increased occurrence  
 198 during a random structure search, the larger volume of this basins can be connected to a higher probability of creating these  
 199 microstates during the PLD growth process. It must be underlined that the amount of sampled structures are not enough to yield  
 200 a quantitative statistical prediction. However, this contained computational effort is sufficient to sketch a qualitative picture, as  
 201 the frequencies of occurrence are due to converge with the number of structures.

202 The data generated by the random structure search can be further analysed by investigating the concentration of minima found  
 203 in certain energy windows. This constitutes a different way of quantifying configurational entropy and can be described by  
 204 means of the entropy forming ability (EFA) formalism<sup>38</sup>. This formalism was introduced to capture the predisposition of a  
 205 material to form high-entropy single-phase crystals by quantifying the number of accessible quasi-degenerate configurations. A  
 206 high EFA value corresponds to a narrow spectrum which implies the possibility of inducing large randomness (i.e. entropy) at  
 207 finite temperature. On the other hand, a wide spectrum (low EFA) is associated with the presence of high energy barriers and  
 208 hence of ordered phases. The EFA can be expressed with the following formula:

$$EFA = \{ \sigma[\text{spectrum}(H_i)]_{T=0K} \}^{-1} \quad (1)$$

$$\sigma(H_x) = \sqrt{\frac{\sum_i g_i (H_i - H_x)^2}{\sum_i g_i - 1}} \quad (2)$$

209 where  $H_i$  and  $g_i$  are the enthalpy and degeneracy of the collected data points.

210 In this work this formalism will be utilised in a different way compared to previous works, where an EFA value characteristic  
 211 of the material is considered. Instead, we calculate the EFA as a continuous function over the whole spectrum to gain insight  
 212 in how the entropy changes in different energy windows. In this context, the EFA becomes a measure of the expected disorder  
 213 in the synthesised material. By studying how this is affected by different conditions, one can infer a pathway to optimise the  
 214 material order. So far we have focused on exploring  $\text{La}_2\text{TiFeO}_6$  stoichiometric phases only. However, in order to consider more  
 215 microstates that might emerge in realistic growth conditions, stoichiometric defects cannot be excluded. This is particularly true  
 216 for overoxidation which might occur not only during growth in oxygen-rich conditions, but also post growth, especially at high  
 217 temperatures during cool down of the sample. Therefore, we also ran structure searches for unit cells with 25 % La vacancies  
 218 ( $\text{La}_{1.5}\text{TiFeO}_6$ ) and for unit cells with 8 % extra oxygen ( $\text{La}_2\text{TiFeO}_{6.5}$ ). In order to make a fair comparison among the different  
 219 stoichiometries, the defect formation energies  $\Delta H_f$  must be considered. If the defects are considered to be charge neutral, the  
 220 defect formation energy can be expressed as:

$$\Delta H_f = H_{\text{def}} - H_0 + \sum n_x (H_x - \mu_x) \quad (3)$$

221 where  $H_{\text{def}}$ ,  $H_0$  and  $H_x$  are the energy of the relaxed supercell containing  $n_x$  defects, the ground state of the perfect system  
 222 and the elemental reference energy, respectively. The chemical potential of the defect  $\mu_{\text{La}}$  and  $\mu_{\text{O}}$  depends on experimental  
 223 conditions, i.e. partial pressure and temperature. In this work, we considered values ranging between two extremes for the  
 224 chemical potentials of lanthanum and oxygens which refer to La-poor ( $\mu_{\text{La}} = -8.89$  eV), La-rich ( $\mu_{\text{La}} = -3.09$  eV), O-poor ( $\mu_{\text{O}} = -3.87$  eV)  
 225 and O-rich ( $\mu_{\text{O}} = 0.00$  eV) conditions, following the work of Taylor et al.<sup>40,41</sup>. Since the chemical potential has a  
 226 large effect on the spectrum, in turn it also affects the EFA as shown in Fig. 4(a). The center panel shows the dependence of the  
 227 EFA in the double-perovskite stability region on  $\mu_{\text{O}}$  and  $\mu_{\text{La}}$ , reflecting their role on the ability of inducing B-site disorder. As  
 228 one can see, the disorder is expected to increase in O-rich and La-poor conditions, as the formation of the considered defects  
 229 becomes more favourable.

230 It should be underlined that both the frequency of occurrence and the EFA do not fully capture the vibrational entropy  
 231 which is crucial to describe high temperatures phenomena. However, when comparing similar competing phases to describe the  
 232 emergence of disorder, the role of the configurational entropy can safely be assumed to be dominating. In the case of  $\text{La}_2\text{TiFeO}_6$ ,  
 233 the phonon dispersion is dominated by the modes associated to Lanthanum vibrations (see Fig. S5) which is reasonably very  
 234 comparable across the competing low-energy phases exhibiting similar volumes and lattice parameters. This yields very similar

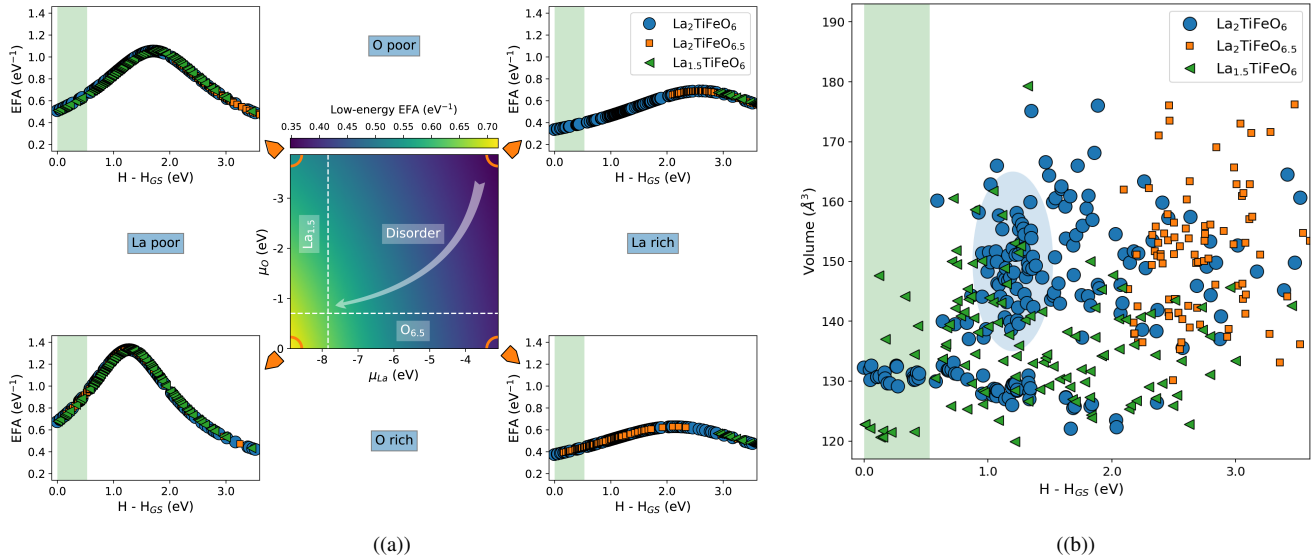


FIG. 4: **(a)** Entropy forming ability analysis of AIRSS results including different stoichiometries in the spectrum. The EFA reflexes the spectrum density and depends on the defect formation energies and hence on the chemical potentials of defects,  $\mu_O$  and  $\mu_{La}$ . This is shown in the central panel where we report the EFA calculated in the energy window of stability for double perovskite structures (0-400 meV). This quantity reflects the amount of disorder that can emerge during material growth. The dashed white lines indicate the values of chemical potential, where the considered defects emerge in this energy window and hence contribute to the disorder. The four corner panels show how the EFA changes as La and O poor and rich conditions are considered. The green area highlights the energy window where perovskite structures are observed. **(b)** Volume distribution of AIRSS results including non-stoichiometric phases in La-poor and O-poor conditions. The blue circle highlights encapsules the region with highest state concentration responsible of the maximum of the EFA. All stoichiometric perovskite phases have comparable volumes of about  $130 \text{ \AA}^3$ . Extra oxygen causes a volume expansion, but phases with similar volumes can be obtained by removing 25 % of La.

235 vibrational contribution for all phases as shown in Fig. S6 for the rock-salt and layered structure, making the configurational  
 236 entropy play a major role to drive disorder.

237 The evolution of the EFA over the energy spectrum is also explored in four corner panels of Fig. 4(a) for four different  
 238 conditions. In all cases, the EFA exhibits a maximum ranging between 1.0-2.5 eV depending on the value of  $\mu_{La}$  and  $\mu_O$ . The  
 239 position of this maximum corresponds to the energy window with the highest configurational entropy, i.e. highest density of  
 240 found minima. As one can see, the effect of  $\mu_{La}$  on the overall EFA is more impactful than  $\mu_O$ . This is because  $\text{La}_{1.5}\text{TiFeO}_6$   
 241 phases are far more spread over the spectrum than  $\text{La}_2\text{TiFeO}_{6.5}$  phases. For practical applications it is important to focus on  
 242 the states more easily accessible from the lowest lying phase. In Fig. 4 we highlight the energy window where the ordered  
 243 perovskites phases reported in Fig. 3 occur, i.e. below 400 meV. It is interesting to note that in this region the EFA increases  
 244 monotonically as a function of the enthalpy and that such increase depends on the chemical potential being steeper in La-poor  
 245 and O-rich conditions. This means that several microstates are condensed in this energy window and hence the entropy is larger,  
 246 possibly causing higher degree of disorder in crystals grown under these conditions.

247 Finally, we explored the structural and magnetic properties of the phases found during the AIRSS search. In Fig. 4(b) we  
 248 report the volume distribution of all minima found by AIRSS in a La-poor and O-poor condition. In the ordered perovskite  
 249 energy window below 400 meV (in green), all phases (see Fig. 3) have comparable volumes around  $130 \text{ \AA}^3$  which is in excellent  
 250 agreement with volumes measured for the films grown on  $\text{SrTiO}_3(100)$  ( $125 \text{ \AA}^3$ ). For the disordered phases above this energy  
 251 window a much broader distribution is observed centered around  $150 \text{ \AA}^3$ . Concerning different stoichiometries, the presence of  
 252 extra oxygens causes a volume expansion and quite a broad distribution with no minima with volumes below  $140 \text{ \AA}^3$ . On the  
 253 other hand, if La vacancies are included several possible structures with comparable volumes (and compressed) to the ordered  
 254 perovskites can be obtained.

255 In order to connect the XPS data presented above to the ab-initio results, we explored the distribution of magnetic moments  
 256 of Fe and Ti ions across the whole spectrum. These are reported in Fig. 5 where the dominance of different oxidations states are  
 257 highlighted, based on the values of the magnetic moments. As it can be seen, titanium cations are non magnetic and hence in the



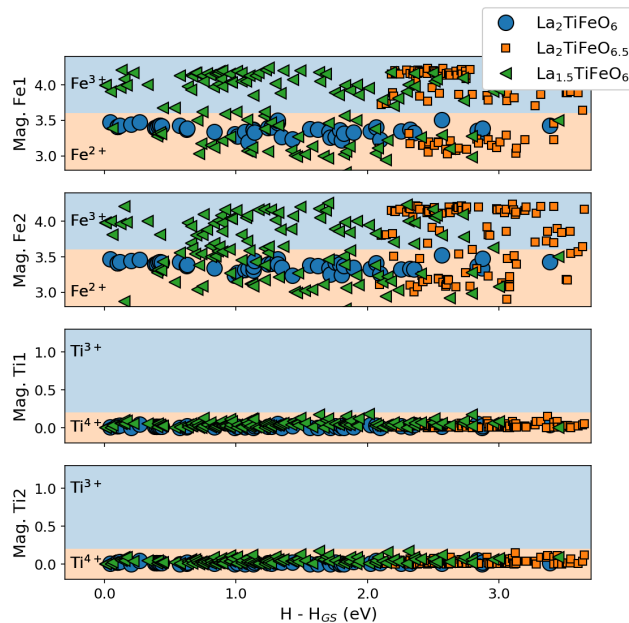


FIG. 5: Magnetic moments distributions from AIRSS results for La-poor and O-poor conditions. The distribution for stoichiometric  $\text{La}_2\text{TiFeO}_6$  is rather homogeneous across the whole spectrum, with the CT  $\text{Fe}^{2+}$  (HS)/ $\text{Ti}^{4+}$  CT state as the most likely state. A higher percentage of oxidised  $\text{Fe}^{3+}$  emerges when defects are included.

258  $\text{Ti}^{4+}$  state for virtually all structures, which fully agrees with XPS data. Similarly, in  $\text{La}_2\text{TiFeO}_6$  iron cations are always in the  
 259  $\text{Fe}^{2+}$  high spin state, but oxidised  $\text{Fe}^{3+}$  species emerge in the other stoichiometries. The local intermixing of non-stoichiometric  
 260 structures with the stoichiometric  $\text{La}_2\text{TiFeO}_6$  phases is therefore probably responsible of the observed  $\text{Fe}^{2+}:\text{Fe}^{3+}$  ratio.

261 More experimental and computational analysis has to be performed in order to conclude which non-stoichiometric phases  
 262 dominate. Presence of lanthanum vacancies (up to 25 %) can be a reasonable explanation, based on similarities between the  
 263 experimental and computed unit cell volumes. However, inclusion of extra oxygen cannot be excluded, since significant amount  
 264 of oxygen can be locally added to the  $\text{La}_2\text{TiFeO}_6$  without destroying the global perovskite structure (see examples in Fig. ??).  
 265 Finally, other non-stoichiometries should be explored too, such as Ti deficient phases or lower defect concentrations based on  
 266 larger computational cells.

267 It is worth stressing the fact that this analysis reflects that non-CT states are extremely unlikely to occur for all stoichiometries  
 268 considered as  $\text{Ti}^{3+}$  states are never found. As pointed out above, this is connected to a reduced volume of the basins of attraction  
 269 and highlights that these states are not easily accessible. This is quite remarkable information that can be obtained by random  
 270 structure sampling methods. Indeed, although we were able to isolate and characterise these states (see Fig. 2) their existence is  
 271 irrelevant for practical applications if they cannot be accessed easily.

## 272 CONCLUSION

273 In this work, we employed an ab-initio random structure search method to address the entropic contributions to B-site disorder  
 274 in double perovskite oxides. High quality  $\text{La}_2\text{TiFeO}_6$  and  $\text{La}_2\text{VCuO}_6$  thin films were grown by Pulsed Laser Deposition, but  
 275 B-site ordering could not be observed. In the case of  $\text{La}_2\text{TiFeO}_6$ , charge transfer from Ti to Fe led to the presence of  $\text{Fe}^{2+}$ .  
 276 However, only part of the Fe was reduced, while Ti was completely oxidized, which is contradictory to the complete charge  
 277 transfer predicted by ab-initio calculations. In order to explain the experimentally observed B-site disorder and oxidation state  
 278 distributions, a random sampling approach was employed including analysis of defects. Combining the analysis of the frequency  
 279 of occurrence of the sampled phases and the entropy forming ability we discussed how the configurational entropy rapidly  
 280 increases above the ground state. The AIRSS search revealed a dense spectrum characterised by several ordered perovskite  
 281 phases within 400 meV above the ground state. Also, exploration of different stoichiometries,  $\text{La}_{1.5}\text{TiFeO}_6$  and  $\text{La}_2\text{TiFeO}_{6.5}$ ,  
 282 yielded a wider overview over the nature of the phases contributing to the observed disorder. The statistically significant phase  
 283 set sampled by AIRSS was used to constructed a thermodynamic model aiming to understand whether the B-site disorder is  
 284 due to an intrinsic competition of different phases and/or if tuning experimental conditions might affect it. The EFA analysis

285 suggested that controlling the partial pressure of oxygen and lanthanum in the chamber might minimise the presence of chemical  
 286 defects, which provides a guide for further experimentation. Nevertheless, the competition of low-energy stoichiometric phases  
 287 appears to be the dominant factor for the B-site disorder which is much harder to control in an experimental set-up. Although  
 288 this work does not provide definitive theory for describing the growth of double perovskites, the described insights into the  
 289 competing phases allowed us to understand the driving force for the observed disorder. The AIRSS study showed presence  
 290 of non-stoichiometric phases can explain the observed large  $\text{Fe}^{3+}:\text{Fe}^{2+}$  ratio, contrary to the expected absence of  $\text{Fe}^{3+}$  for  
 291 stoichiometric phases. This work shows the value of high-throughput ab-initio calculations to investigate formation of realistic  
 292 but imperfect materials.

## 293 METHODS

### 294 Experimental setup

295 45 monolayers  $\text{La}_2\text{TiFeO}_6$  and 30 monolayers  $\text{La}_2\text{VCuO}_6$  epitaxial films were synthesised on  $\text{TiO}_2$  terminated single-  
 296 crystalline  $\text{SrTiO}_3(001)$  and  $\text{SrTiO}_3(111)$  substrates from stoichiometric ceramic targets via pulsed-laser deposition (248 nm  
 297 KrF laser). The deposition temperatures of  $\text{La}_2\text{TiFeO}_6$  and  $\text{La}_2\text{VCuO}_6$  were 730 °C and 700 °C respectively, in an oxygen  
 298 pressure of  $2 \times 10^{-6}$  Torr. For all materials, the laser fluence was 1.0 J/cm<sup>2</sup>, while a laser repetition rate of 1 Hz was used.  
 299 Reflection high-energy electron diffraction (RHEED) was used during the deposition to ensure a layer-by-layer growth mode.  
 300 After deposition, the films were cooled down to room temperature at the oxygen pressure used during growth. Structural char-  
 301 acterisation of the films were carried out using a Panalytical X'Pert Pro X-ray Diffraction (XRD) diffractometer with  $\text{Cu-K}\alpha$   
 302 radiation ( $\lambda=1.5405 \text{ \AA}$ ). The high crystalline quality of the films was confirmed from  $\theta - 2\theta$  symmetric XRD scans around the  
 303 (002) reflections. The lattice parameters and the tetragonal symmetry are calculated from reciprocal space maps (RSMs) around  
 304 the (103) reflections. Ex-situ XPS measurements were performed on a PHI VersProbe 3 using monochromated  $\text{Al-K}\alpha$  radiation.  
 305 The TEM measurements were performed at a Cs probe-corrected FEI TITAN operating at 200 kV equipped with a Fischione  
 306 HAADF detector. The cross-sectional samples were prepared using standard mechanical polishing and dimpling techniques  
 307 with a final polishing in a Gatan PIPS ion mill using a 3 kV argon beam.

### 308 Computational details

309 All DFT calculations were performed within the Quantum Espresso code (version 6.5) employing the PBE functional and the  
 310 Hubbard- $U$  local correction in the  $d$ -shells of the transition metals. The values for the Ti and Fe were chosen in accordance to  
 311 the vast literature on DFT+ $U$  for similar materials, *i.e.*  $U(\text{Ti}) = 3.0 \text{ eV}$ ,  $U(\text{Fe}) = 4.8 \text{ eV}$ . For  $\text{La}_2\text{VCuO}_6$  our choice of  $U$ -values  
 312 differs from the referred literature values as they were obtained by means of the self-consistent linear response density functional  
 313 perturbation theory (DFPT) method proposed by Cococcioni et al.<sup>42</sup> as implemented in Quantum Espresso. The  $U$  on vanadium  
 314 was found to be practically indifferent to the 4+/5+ oxidation states, yielding values of 3.5-4.0eV. On the other hand, the  $U$   
 315 obtained on  $\text{Cu}^{2+}$  was around 8.0 eV, while it was undefined for  $\text{Cu}^+$ . This is due to a well known issue with the linear response  
 316 approach when the correction is applied to filled d-shells. However, since both the energy and the DOS of the non-magnetic state  
 317 is not strongly dependent on the choice of  $U$ , we settled to values of 8.0 eV for a fairer comparison. Plane-wave basis set with an  
 318 energy cut-off of 800 eV and a  $4 \times 4 \times 3$   $k$ -mesh were used with ultrasoft pseudopotentials (USPP) to describe the atomic cores  
 319 with valence configurations  $\text{La}(4f\ 5s\ 5p\ 5d\ 6s\ 6p)$ ,  $\text{Ti}(3s\ 3p\ 4s\ 3d)$ ,  $\text{Fe}(3s\ 3p\ 3d\ 4s\ 4p)$ ,  $\text{V}(3s\ 3p\ 4s\ 3d)$ ,  $\text{Cu}(3s\ 3p\ 3d\ 4s\ 4p)$  and  
 320  $\text{O}(2s\ 2p)$ . All calculations were converged to energy  $<0.1 \text{ meV}$  and force  $<1.0 \text{ meV \AA}^{-1}$ .

321 In order to model the growth of the films on different substrates we constrained the surface vectors in accordance to the  
 322 substrate parameters and allowed for the relaxation along the growth direction as well as of internal coordinates. The initial  
 323 internal coordinates were chosen to represent the bulk  $Pnma$  spacegroup symmetry of  $\text{LaFeO}_3$ ,  $\text{LaVO}_3$  and  $\text{LaTiO}_3$  with oc-  
 324 tahedral rotations  $a^-b^-c^+$ . In order to study the effect of B-site in these double perovskites we investigated both the layered  
 325 and rock-salt order in different magnetic orientations. As the magnetic orientations of all the building blocks is G-type, it is  
 326 reasonable to believe that it will be maintained also in the heterostructures. It has to be pointed out that in the case of  $\text{La}_2\text{VCuO}_6$   
 327 the situation is not as clear, since  $\text{LaCuO}_3$  has never been observed experimentally and ab-initio studies debate whether or not it  
 328 is non-magnetic with a formally  $\text{Cu}^{3+}$  in a  $d^9$ -L state<sup>43-45</sup>.

329 The AIRSS package interfaced with Quantum Espresso was used for the random structure sampling. All searches were  
 330 performed at 0 GPa, targeting an initial volume of about  $125 \text{ \AA}^3 \pm 20\%$ . Distance constraints were imposed by loosening of 20%  
 331 the interatomic distances in an ordered  $\text{LaFeO}_3$  perovskite. This allowed to explore a vast number of random sensible structures  
 332 while respecting the relevant chemistry expected in double perovskites. The ab-initio DFT calculations were performed by  
 333 sampling on a grid of spacing  $2\pi \times 0.1^{-1}$  and a plane-wave basis set cutoff of 500 eV. The final structures were further  
 334 relaxed at the higher level of accuracy reported above. The samplings for  $\text{La}_2\text{TiFeO}_6$ ,  $\text{La}_2\text{TiFeO}_{6.5}$  and  $\text{La}_{1.5}\text{TiFeO}_6$  were run  
 335 separately employing cells consisting 2 formula units imposing random space groups with 2 to 4 symmetry elements. The

336 starting magnetic moments of Ti and Fe ions were also randomly generated. Via the AIRSS sampling a total of 400 random  
337 structures were obtained.

338 In order to test for long-range ordering phenomena, we constructed cells of 4 formula units by elongating the stoichiometric  
339 ground state 2 formula unit cell along all lattice vectors, in turn and applying random displacements of the atomic positions up  
340 to 0.1 Å. In all cases, the structural relaxations lead to the same minima identified for the smaller cell with energy differences  
341 below  $10^{-7}$  eV. Although it would be computationally prohibiting to test this for all phases and stoichiometry considered, the  
342 absence of new superstructures in the ground state justify the size for the cell considered.

### 343 DATA AVAILABILITY

344 The data that support the findings of this study are available from the corresponding author upon reasonable request.

### 345 REFERENCES

- 346 <sup>1</sup>C. A. López, J. C. Pedregosa, D. G. Lamas, and J. A. Alonso, “The strongly defective double perovskite  $\text{Sr}_{11}\text{Mo}_4\text{O}_{23}$ : Crystal structure in relation to ionic  
347 conductivity,” *Journal of Applied Crystallography* **47**, 1395–1401 (2014).
- 348 <sup>2</sup>M. H. K. Rubel, A. Miura, T. Takei, N. Kumada, M. Mozahar Ali, M. Nagao, S. Watauchi, I. Tanaka, K. Oka, M. Azuma, E. Magome, C. Moriyoshi,  
349 Y. Kuroiwa, and A. K. M. Azharul Islam, “Superconducting Double Perovskite Bismuth Oxide Prepared by a Low-Temperature Hydrothermal Reaction,”  
350 *Angewandte Chemie* **126**, 3673–3677 (2014).
- 351 <sup>3</sup>T. Chakraborty, H. S. Nair, H. Nhalil, K. Ramesh Kumar, A. M. Strydom, and S. Elizabeth, “Disordered ferromagnetism in  $\text{Ho}_2\text{NiMnO}_6$  double perovskite,”  
352 *Journal of Physics Condensed Matter* **29** (2017), 10.1088/0953-8984/29/2/025804.
- 353 <sup>4</sup>M. Hashisaka, D. Kan, A. Masuno, M. Takano, Y. Shimakawa, T. Terashima, and K. Mibu, “Epitaxial growth of ferromagnetic  $\text{La}_2\text{NiMnO}_6$  with ordered  
354 double-perovskite structure,” *Applied Physics Letters* **89** (2006), 10.1063/1.2226997.
- 355 <sup>5</sup>T. Fukushima, A. Stroppa, S. Picozzi, and J. M. Perez-Mato, “Large ferroelectric polarization in the new double perovskite  $\text{NaLaMnWO}_6$  induced by  
356 non-polar instabilities,” *Physical Chemistry Chemical Physics* **13**, 12186–12190 (2011), arXiv:1104.5099.
- 357 <sup>6</sup>G. Gou, N. Charles, J. Shi, and J. M. Rondinelli, “A-Site Ordered Double Perovskite  $\text{CaMnTi}_2\text{O}_6$  as a Multifunctional Piezoelectric and Ferroelectric-  
358 Photovoltaic Material,” *Inorganic Chemistry* **56**, 11854–11861 (2017).
- 359 <sup>7</sup>Y. Shimakawa, M. Azuma, and N. Ichikawa, “Multiferroic compounds with double-perovskite structures,” *Materials* **4**, 153–168 (2011).
- 360 <sup>8</sup>C. Gauvin-Ndiaye, A.-M. S. Tremblay, and R. Nourafkan, “Electronic and magnetic properties of the double perovskites  $\text{La}_2\text{MnRuO}_6$  and  $\text{LaAMnFeO}_6$   
361 ( $a=\text{Ba,Sr,Ca}$ ) and their potential for magnetic refrigeration,” *Phys. Rev. B* **99**, 125110 (2019).
- 362 <sup>9</sup>T. Saha-Dasgupta, “Double perovskites with 3d and 4d/5d transition metals: compounds with promises,” *Materials Research Express* **7**, 014003 (2020).
- 363 <sup>10</sup>M. A. Chen, H., “Design of new mott multiferroics via complete charge transfer: promising candidates for bulk photovoltaics,” *Sci. Rep.* **7**, 6142 (2017).
- 364 <sup>11</sup>S. R. Spurgeon, Y. Du, T. Droubay, A. Devaraj, X. Sang, P. Longo, P. Yan, P. G. Kotula, V. Shutthanandan, M. E. Bowden, J. M. LeBeau, C. Wang, P. V.  
365 Sushko, and S. A. Chambers, “Competing pathways for nucleation of the double perovskite structure in the epitaxial synthesis of  $\text{La}_2\text{MnNiO}_6$ ,” *Chemistry of*  
366 *Materials* **28**, 3814–3822 (2016), <https://doi.org/10.1021/acs.chemmater.6b00829>.
- 367 <sup>12</sup>V. Shabadi, M. Major, P. Komissinskiy, M. Vafaee, A. Radetinac, M. Baghaie Yazdi, W. Donner, and L. Alff, “Origin of superstructures in (double) perovskite  
368 thin films,” *Journal of Applied Physics* **116**, 114901 (2014), <https://doi.org/10.1063/1.4895636>.
- 369 <sup>13</sup>S. Vasala and M. Karppinen, “ $\text{A}_2\text{BBO}_6$  perovskites: A review,” *Progress in Solid State Chemistry* **43**, 1 – 36 (2015).
- 370 <sup>14</sup>G. King and P. M. Woodward, “Cation ordering in perovskites,” *J. Mater. Chem.* **20**, 5785–5796 (2010).
- 371 <sup>15</sup>A. Ohtomo, S. Chakraverty, H. Mashiko, T. Oshima, and M. Kawasaki, “Spontaneous atomic ordering and magnetism in epitaxially stabilized double  
372 perovskites,” *Journal of Materials Research* **28**, 689–695 (2013).
- 373 <sup>16</sup>H. Chen and A. Millis, “Antisite defects at oxide interfaces,” *Phys. Rev. B* **93**, 104111 (2016).
- 374 <sup>17</sup>H. Chen and A. Millis, “Charge transfer driven emergent phenomena in oxide heterostructures,” *Journal of Physics: Condensed Matter* **29**, 243001 (2017).
- 375 <sup>18</sup>C. Lupo, E. Sheridan, E. Fertitta, C. Pickard, D. Dubbink, and C. Weber, “Tuning the strength of electronic correlations by epitaxial engineering : From slater  
376 to mott physics in a geological state of iron induced by charge transfer,” (To be published).
- 377 <sup>19</sup>V. Pardo and W. E. Pickett, “Evaluation of compensated magnetism in  $\text{La}_2\text{VCuO}_6$ : Exploration of charge states,” *Phys. Rev. B* **84**, 115134 (2011).
- 378 <sup>20</sup>J. E. Kleibeuker, E.-M. Choi, E. D. Jones, T.-M. Yu, B. Sala, B. A. MacLaren, D. Kepaptsoglou, D. Hernandez-Maldonado, Q. M. Ramasse, L. Jones,  
379 J. Barthel, I. MacLaren, and J. L. MacManus-Driscoll, “Route to achieving perfect b-site ordering in double perovskite thin films,” *NPG Asia Mater* **9**, e406  
380 (2017).
- 381 <sup>21</sup>A. R. Oganov and C. W. Glass, “Crystal structure prediction using ab initio evolutionary techniques: Principles and applications,” *Journal of Chemical Physics*  
382 **124** (2006), 10.1063/1.2210932.
- 383 <sup>22</sup>Y. Wang, J. Lv, L. Zhu, and Y. Ma, “Crystal structure prediction via particle-swarm optimization,” *Physical Review B - Condensed Matter and Materials*  
384 *Physics* **82**, 1–8 (2010), arXiv:1008.3601.
- 385 <sup>23</sup>A. O. Lyakhov, A. R. Oganov, H. T. Stokes, and Q. Zhu, “New developments in evolutionary structure prediction algorithm USPEX,” *Computer Physics*  
386 *Communications* **184**, 1172–1182 (2013).
- 387 <sup>24</sup>A. R. Oganov, A. O. Lyakhov, and M. Valle, “How evolutionary crystal structure prediction works-and why,” *Accounts of Chemical Research* **44**, 227–237  
388 (2011).
- 389 <sup>25</sup>Y. Wang, J. Lv, L. Zhu, and Y. Ma, “CALYPSO: A method for crystal structure prediction,” *Computer Physics Communications* **183**, 2063–2070 (2012).
- 390 <sup>26</sup>A. R. Oganov, C. J. Pickard, Q. Zhu, and R. J. Needs, “Structure prediction drives materials discovery,” *Nature Reviews Materials* **4**, 331–348 (2019).
- 391 <sup>27</sup>A. F. Harper, M. L. Evans, J. P. Darby, B. Karasulu, C. P. Koçer, J. R. Nelson, and A. J. Morris, “Ab initio structure prediction methods for battery materials a  
392 review of recent computational efforts to predict the atomic level structure and bonding in materials for rechargeable batteries,” *Johnson Matthey Technology*  
393 *Review* **64**, 103–118 (2020).
- 394 <sup>28</sup>C. J. Pickard and R. J. Needs, “Ab initio random structure searching,” *Journal of Physics Condensed Matter* **23** (2011), 10.1088/0953-8984/23/5/053201,  
395 arXiv:1101.3987.

- 396 <sup>29</sup>C. J. Pickard and R. J. Needs, “Structure of phase III of solid hydrogen,” *Nature Physics* **3**, 473–476 (2007).
- 397 <sup>30</sup>C. J. Pickard and R. J. Needs, “Highly compressed ammonia forms an ionic crystal,” *Nature Materials* **7**, 775–779 (2008).
- 398 <sup>31</sup>A. Reinhardt, C. J. Pickard, and B. Cheng, “Predicting the phase diagram of titanium dioxide with random search and pattern recognition,” *Physical Chemistry*
- 399 *Chemical Physics* **22**, 12697–12705 (2020), arXiv:1909.08934.
- 400 <sup>32</sup>V. Stevanović, “Sampling Polymorphs of Ionic Solids using Random Superlattices,” *Physical Review Letters* **116**, 1–5 (2016).
- 401 <sup>33</sup>C. J. Bartel, S. L. Millican, A. M. Deml, J. R. Rumpitz, W. Tumas, A. W. Weimer, S. Lany, V. Stevanović, C. B. Musgrave, and A. M. Holder, “Physical descriptor for the Gibbs energy of inorganic crystalline solids and temperature-dependent materials chemistry,” *Nature Communications* **9** (2018), 10.1038/s41467-018-06682-4, arXiv:1805.08155.
- 402 <sup>34</sup>E. B. Jones and V. Stevanović, “Polymorphism in elemental silicon: Probabilistic interpretation of the realizability of metastable structures,” *Physical Review*
- 403 *B* **96**, 1–8 (2017), arXiv:1708.09026.
- 404 <sup>35</sup>S. V. Krivovichev, “Structural complexity and configurational entropy of crystals,” *Acta Crystallographica Section B: Structural Science, Crystal Engineering*
- 405 *and Materials* **72**, 274–276 (2016).
- 406 <sup>36</sup>V. N. Manoharan, “Colloidal matter: Packing, geometry, and entropy,” *Science* **349** (2015), 10.1126/science.1253751.
- 407 <sup>37</sup>B. A. Wilson, A. T. Nasrabadi, L. D. Gelb, and S. O. Nielsen, “Computing free energies using nested sampling-based approaches,” *Molecular Simulation* **44**,
- 408 1108–1123 (2018).
- 409 <sup>38</sup>P. Sarker, T. Harrington, C. Toher, C. Oses, M. Samiee, J. P. Maria, D. W. Brenner, K. S. Vecchio, and S. Curtarolo, “High-entropy high-hardness metal
- 410 carbides discovered by entropy descriptors,” *Nature Communications* **9**, 1–10 (2018), arXiv:1811.07730.
- 411 <sup>39</sup>J. E. Kleibecker, Z. Zhong, H. Nishikawa, J. Gabel, A. Müller, F. Pfaff, M. Sing, K. Held, R. Claessen, G. Koster, and G. Rijnders, “Electronic reconstruction
- 412 at the isopolar LaTiO<sub>3</sub>/LaFeO<sub>3</sub> interface: An x-ray photoemission and density-functional theory study,” *Phys. Rev. Lett.* **113**, 237402 (2014).
- 413 <sup>40</sup>F. H. Taylor, J. Buckeridge, and C. R. A. Catlow, “Defects and oxide ion migration in the solid oxide fuel cell cathode material LaFeO<sub>3</sub>,” *Chemistry of*
- 414 *Materials* **28**, 8210–8220 (2016).
- 415 <sup>41</sup>F. H. Taylor, J. Buckeridge, and C. R. A. Catlow, “Screening Divalent Metals for A- and B-Site Dopants in LaFeO<sub>3</sub>,” *Chemistry of Materials* **29**, 8147–8157
- 416 (2017).
- 417 <sup>42</sup>M. Cococcioni and S. De Gironcoli, “Linear response approach to the calculation of the effective interaction parameters in the LDA+U method,” *Physical*
- 418 *Review B - Condensed Matter and Materials Physics* **71**, 1–16 (2005), arXiv:0405160 [cond-mat].
- 419 <sup>43</sup>T. Mizokawa, H. Namatame, A. Fujimori, K. Akeyama, H. Kondoh, H. Kuroda, and N. Kosugi, “Origin of the band gap in the negative charge-transfer-energy
- 420 compound NaCuO<sub>2</sub>,” *Physical Review Letters* **67**, 1638–1641 (1991).
- 421 <sup>44</sup>Y. Nohara, S. Yamamoto, and T. Fujiwara, “Electronic structure of perovskite-type transition metal oxides LaM O<sub>3</sub> (M=TiCu) by U+GW approximation,”
- 422 *Physical Review B - Condensed Matter and Materials Physics* **79**, 1–14 (2009).
- 423 <sup>45</sup>J. He and C. Franchini, “Screened hybrid functional applied to 3d03d8 transition-metal perovskites LaMO<sub>3</sub> (M=Sc-Cu): Influence of the exchange mix-
- 424 ing parameter on the structural, electronic, and magnetic properties,” *Physical Review B - Condensed Matter and Materials Physics* **86**, 1–33 (2012),
- 425 arXiv:1209.0486.
- 426
- 427

## 428 ACKNOWLEDGMENTS

429 Part of this work was performed at the Stanford Nano Shared Facilities (SNSF), supported by the National Science Founda-

430 tion under award ECCS-1542152. CW was supported by grant EP/R02992X/1 from the UK Engineering and Physical Sciences

431 Research Council (EPSRC). This work was performed using resources provided by the ARCHER UK National Supercomput-

432 ing Service and the Cambridge Service for Data Driven Discovery (CSD3) operated by the University of Cambridge Research

433 Computing Service (www.csd3.cam.ac.uk), provided by Dell EMC and Intel using Tier-2 funding from the Engineering and

434 Physical Sciences Research Council (capital grant EP/P020259/1), and DiRAC funding from the Science and Technology Fa-

435 cilities Council (www.dirac.ac.uk). CW and DB are grateful to Antoine George, Nicola Bonini and Francesco Macheda for

436 insightful discussions. CJP acknowledges the support of a Royal Society Wolfson Research Merit award. EF and DB thank

437 Matteo Cocconi and Iurii Timrov for useful insights.

## 438 AUTHOR CONTRIBUTIONS

439 R.R., C.W., D.D., C.J.P., C.B. and P.L. designed research; E.F., S.D., D.B., F.E., K.D. and H.T. performed research; E.F.,

440 D.D., S.D. and F.E. analysed data; S.D. synthesized and prepared samples; and E.F. and D.D. wrote the paper with input from

441 all the authors.

## 442 COMPETING INTERESTS

443 The authors declare no competing interest.